Article:
Demiryurek, S.G. and Krynkin, A. (2026) Low-frequency resonators filled with granular material for modal response treatment. Journal of Low Frequency Noise Vibration and Active Control. ISSN: 0263-0923

https://doi.org/10.1177/14613484261423623

Original research manuscript

Journal of LOW FREQUENCY NOISE, VIBRATION AND ACTIVE CONTROL

Journal of Low Frequency Noise, Vibration and Active Control
2026, Vol. 0(0) 1–17

DOI: 10.1177/14613484261423623
journals.sagepub.com/home/lfn
Sage

Low-frequency resonators filled with granular material for modal response treatment

Sifa Gul Demiryurek[1] and Anton Krynkin[2]

Abstract

Resonators are commonly employed as passive dampers to suppress structural vibrations. This study proposes a novel resonator concept designed for low-frequency control of a host structure, incorporating a granular-filled cavity to enhance damping and enable tunability of the target modal response. The resonator can be manufactured using additive techniques, and its resonant behaviour is estimated empirically from its geometry and material properties. The effect of multiple resonators on the modal response of the main structure is shown numerically and experimentally offering wider attenuation frequency bandwidth where bending modes of the main structure are successfully controlled. Incorporating only 10% volume fraction of granular material in resonator that have a negligible effect on its overall mass yields an additional 45% damping improvement and expands the effective attenuation bands.

Keywords

vibration damping, resonance, local resonators, coupling, tuned resonators, particle damper

Introduction

Structural vibration can significantly affect structures and machine parts, resulting in a shortened service life, reduced precision and performance, and increased dynamic stress on the structures. These outcomes lead to fatigue and wear, necessitating immediate and sudden maintenance. Specifically, low-frequency vibrations are particularly hazardous due to their long wavelength, which enables them to affect larger areas of the structure. Efforts to mitigate the effects of structural vibration have been ongoing for many years, involving the exploration of various damping options.[1]

Vibration impacts can be managed through several approaches: designing low-vibration structures, isolating the vibration path, creating opportunities for vibration energy absorption, and isolating the receiving structure from the vibration impacts.[2] The creation of low-vibration structures can be challenging due to complex manufacturing requirements. Additionally, protecting the structural components becomes impossible when the receiving structure exhibits active movement.[3] Therefore, the most practical option in such applications is to develop dynamic load dampers which dampen the structural energy while providing specific dynamic properties, such as built-in local resonator. Although these solutions mitigate the effects of structural vibration, they have limitations when applied. For example, passive dampers are limited in their design properties and dynamic aspects, as they are tailored to be effective only under specific operating conditions.[4] On the other hand, placing locally resonating structures along the vibration path in specific arrangements like periodic order helps control structural vibration by harnessing excess energy from the main structure to achieve resonance. These structures counteract excitation impacts and function as vibration dampers; specifically, when the resonance frequency closely matches the excitation frequency. A single resonator

[1]Department of Mechanical Engineering, Aksaray University, Aksaray, Türkey
[2]Department of Mechanical Engineering, The University of Sheffield, Sheffield, UK

Corresponding author:
Sifa Gul Demiryurek, Department of Mechanical Engineering, Aksaray University, Bahçesaray Mah. 171. Cad. No:10, Merkez, Aksaray 68100, Türkey.
Email: sgdemiryurek@aksaray.edu.tr

attachment exhibits eigenfrequency modulation impact on the main substrate, while resonators arranged in multiples demonstrate coupled structural behaviours which both control the dynamic properties and provide wider frequency response treatment.[5]

In cases involving undamped dynamic vibration absorbers as local resonators, a resonator attached to the main structure splits the frequency peak. On the other hand, in damped dynamic vibration cases, the presence of damping in the resonator reduces the amplitudes received from the main structure in addition to the effect produced by absorber with no damping properties. According to Pai,[6] controlling the structural vibration using array of resonating structures is more efficient leveraging strong coupling and energy absorption properties than using single resonator attachments. On the other hand, the additional damping characteristics of the local resonators contributed to modulation of the amplitude of the frequency response while providing stop frequency band.[5]

Periodically placed local resonators behave as mechanical filter by passing or blocking the frequency propagation according to their dynamic features and coupling properties.[7] Therefore, periodically arranged local resonators, known as metamaterials, provide frequency band properties such as stop and pass bands.[8] Consequently, the metamaterial[9] dissipates mechanical energy in both high and low frequency ranges. The periodic array of resonators is usually investigated through modelling of a unit cell by defining specific boundary conditions; like Bloch-Floquet Conditions; which makes them as infinitely long structures and enables investigating the stop and pass bands.[10–12]

In this study the mechanical metamaterials as a concept of the structural vibration dampers is further advanced by integrating granular medium with the dampers. These granules are placed within the damper cavity with the purpose of converting structural vibration energy into momentum exchanges within the granular medium. While the main structure is under excitation impact, upcoming kinetic energy is ultimately absorbed and transformed into the momentum changes within the granules through two impact interactions: particle–particle and particle–damper wall impact interactions that are inelastic collisions.[4] This conversion helps balance momentum exchanges and ultimately reduces amplitude of structural vibration experienced by the host structure and is essentially creating a particle damper.[13] It is crucial that the granular bodies within the damper cavity have effective contact interactions, and the cavity should have smooth walls and no sharp edges,[14] as is the case with a sphere-shaped geometry.

Following the principles of vibration damping, this research aims to mitigate structural vibration of the main substrate using dynamic absorbers designed to resonate at frequency below 1000 Hz.[15,16] The dynamic absorbers are usually designed based on the idea of lumped mass–spring system.[17] This study offers a novel approach to the design of the resonator where resonance is defined by the geometry and material properties of its solid structure. The resonator design includes a cavity where the granules can be placed to convert structural vibration energy into momentum exchanges within the granular medium while aiming to tune the resonators. The resonator incorporates a spherical void to increase the likelihood of contact and collisions among granular structures. This enables us to compare the theoretical results with the experiment based on the laboratory-scale setup of the beam which exhibits its dominant measurable mode at around 760 Hz. It should be noted that the resonator concept is fully scalable to lower frequencies typically encountered in engineering systems. This study seeks to introduce an innovative approach to the modelling and design of the resonator, enabling its application not only as a locally resonating structure within a periodic arrangement but also as a host framework for granular bodies. A key contribution of this research is the development of a novel resonating structure that integrates locally resonating granular dampers, representing a significant advancement in the field.

The proposed granular-filled low-frequency resonators differ fundamentally from conventional mass–spring locally resonant attachments widely reported in the literature, including the multi-resonator configurations described by Pai and co-workers.[18] In classical single mass–spring absorbers, attenuation relies purely on linear resonance tuning; therefore, the achievable bandwidth is inherently narrow, and performance degrades if excitation conditions deviate from the design frequency. In contrast, the granular-filled resonators examined in this study introduce additional amplitude-dependent energy dissipation through particle–particle and particle–wall interactions. This nonlinear mechanism results in a broader attenuation region and improved robustness compared with purely elastic mass–spring resonators attached to the host structure. The present work, therefore, extends the classical locally resonant framework by combining resonance-based response shaping with granular damping, demonstrating a hybrid mechanism that yields wider and more stable vibration suppression than reported in traditional mass–spring resonator studies such as those of Pai.[18]

The structure of the paper is as follows: firstly, an innovative design procedure for locally resonating structures is outlined in section of Low-frequency Resonator. Then the FRF of the main structure with single and multiple resonators are investigated with the help of FEM in section of Finite Element Modelling of Beam-Resonator System. The numerical cases for single and multiple resonators are validated experimentally in section of Experiment. In the last section of this paper, section of Resonators Partially Filled with Granular Material, cavity-based resonators are filled with granular medium with 10% of

the cavity volume of the resonator to experimentally prove benefits of the granular medium effect combined with the impact of the resonator.

Low-frequency resonator

In this study, the main structure is assumed to be a solid beam with rectangular cross-section. The beam is fixed at both ends and has slits along its length for mounting the resonators as shown in Figure 1. The dimensions and material properties of the beam are given in Table 1.

Commercial software COMSOL Multiphysics version 5.1 is employed to model structural vibration in this study. The numerical simulations based on Finite Element Method (FEM) have been run on workstation with Intel(R) Xeon(R) CPU with 128 GB RAM. The material parameters used in the finite element model correspond to structural steel as defined in the COMSOL Multiphysics version 5.1 material library. For the dimensions and material properties shown in Table 1, the beam exhibits the first three bending modes at around the following frequencies 140 Hz, 420 Hz, and 760 Hz according to the numerical simulation. The particular focus of this research is on the third bending mode of the beam (at around 760 Hz) in the vicinity of which it is possible to tune the performance of the resonator introduced in the title of Finite Element Modelling of the Resonator. This enables us to compare the theoretical results with the experiment based on the laboratory-scale setup of the beam which exhibits its dominant measurable mode at around 760 Hz. It should be noted that the resonator concept is fully scalable to lower frequencies typically encountered in engineering systems.

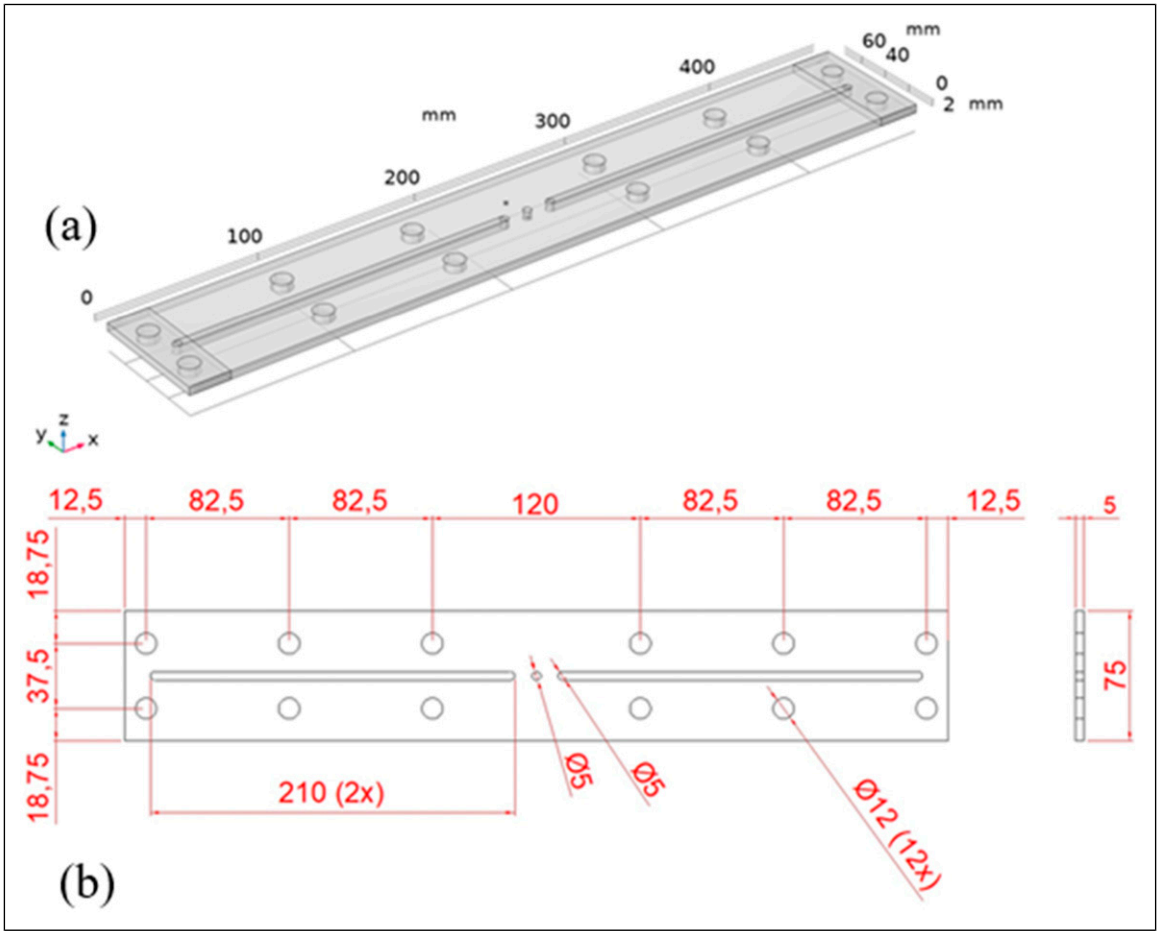

Figure 1. The main structure (the bare beam) representation with the mounting holes as seen in COMSOL (a) and precise dimensions (b).

Table 1. Material properties and the geometric details of the main structure.

Material properties	Young's modulus [Pa]	200E+09
	Poisson's ratio [-]	0.33
	Density [kg/m^3]	7850
Geometric details	Length [mm]	475
	Thickness [mm]	5
	Width [mm]	75

Material properties of 3D-printed resonator

The resonator introduced in the title of Finite Element Modelling of the Resonator is constructed using the 3D-printing technique. In this manufacturing technique, structures are built layer by layer, leading to some level of porosity within the printed structure which leads to changes in the sample's material and mechanical properties.[19] Therefore, the use of filament material in the 3D printing does not necessarily mean that the printed structure possesses the filament's properties. This process necessitates a material characterisation test to account for variations in material properties due to factors such as infill ratio, which is a natural consequence of 3D printing.[11,20] To determine the material properties (i.e. Young's modulus, stiffness, and loss properties) of the printed structure, a Dynamic Mechanical Analysis (DMA) testing procedure[21] has been employed[22] using the Metravib Viscoanalyser (Metravib Xpander VA 2000, shown in Figure 2 with an applied dynamic strain of 0.001. Incremental steps of five units have been studied for frequency ranging from 5 to 100 Hz. Each variation in frequency parameter has been evaluated through the tension-compression test under sinusoidal stress impacts. As the experimental analysis in this study has been conducted in a room environment, the ambient temperature for assessing material properties has been hold constant at 25°C.

To conduct the DMA test, a sample measuring 20 mm × 10 mm × 10 mm, made of ABS (Acrylonitrile Butadiene Styrene), was 3D-printed with the 65% infill ratio using the Ultimaker Cura 3D-printing machine. Figure 3 illustrates the prismatic specimen used exclusively for DMA-based material characterisation. It should be noted that this specimen is not a resonator and the actual resonator geometry has cylindrical and spherical sections in one body, as shown in Figure 4. In general, ABS offers lower rigidity but results in light structures,[23] making it a suitable material for this research. The density of the sample was measured as 950 kg/m^3, using the volume and the mass of the printed sample. Due to the relatively low density, the complete 3D-printed resonator's mass was around 33 g, making them much lighter than the beam itself (approximately 1.5 kg).

Based on the DMA measurements, Young's modulus shows only a slight change which is less than 3% across the 5–100 Hz test range, indicating that the material exhibits negligible stiffness–frequency dependence within this interval. In the finite element simulations and experimental analyses in this study the material was treated as effectively frequency-independent over the operational bandwidth. Young's modulus and loss factor used in the numerical model and shown in Table 2 corresponds to the 100 Hz value, representing the upper bound of the DMA measurement.

Finite element modelling of the resonator

The geometry of the resonator adopts a spherical-hollow shape mounted on the solid cylindrical support. The cylindrical shape of the support is selected for the convenience to assemble support with the sphere.

In this study, the hollow sphere and cylinder form a single solid structure joined at the top of the cylindrical support as shown in Figure 4. The contact area between the sphere and cylindrical base has been used to control the resonator's natural frequencies and the area defines the stiffness of the structure drawing similarity with the mass–spring–mass connection.[7] In particular, the contact area between the upper and the lower part of the resonating structure has been compared to the spring element. The radii of the hollow section of the sphere and the cylinder as well as the height of the base can be differentiated to vary the natural frequency of the resonator. In order to avoid ambiguity in the analyses, all geometric parameters were explicitly categorised, with the base height, inner radius, and outer radius of the sphere defined as fixed parameters, whereas the cylindrical-spherical contact length, and radius of the base were treated as variable parameters. The material properties of the resonator are assumed to be fixed in this study. It should be noted that changing the material at the sphere and cylindrical base interface impacts stiffness of the resonator and its natural frequencies. Due to the selected manufacturing process, the effect of the material on the resonant behaviour is outside of the scope of this study. The resonator consists of a separately printed spherical cavity and its cylindrical support, as

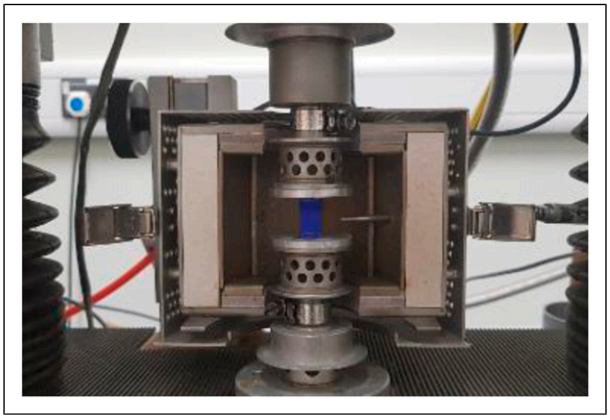

Figure 2. The DMA test machine with the sample placed on the test machine.

mentioned above, which are bonded together prior to the installation. The assembled resonator is then mounted into the beam through the longitudinal slit (shown in Figure 1) via screw fastening.

Numerical simulation has been conducted to investigate the effect of the resonator geometry on its performance. The sphere has been modelled with the inner radius fixed at $R = 20$ mm and a wall thickness equal to $h_t = 5$ mm. The primary parameter for the cylindrical support is the radius of the cylinder R_b. The height of the base is fixed at $L = 35$ mm. The maximum characteristic size of the contact volume formed between the cylindrical support and the sphere has been limited by the diameter of the cylindrical base. Calculation of the maximum contact height, denoted as h_{max}, which is the maximum value of h shown in Figure 4, has been determined using circular segment calculations for the sphere cross-section, yielding

$$h_{max} = \widehat{R} - \sqrt{\widehat{R}^2 - R_b^2}, \tag{1}$$

where $\widehat{R}$ is external radius of the hollow sphere.

This parameter is used to constrain sphere displacement h into the cylindrical base when analysing natural frequencies of the resonator. The height of the cylindrical support L is bigger than h_{max}.

The numerical results have been obtained for four cylindrical bases: (i) $R_b = 5.5\,mm$, (ii) $R_b = 11\,mm$, (iii) $R_b = 25\,mm$, and (iv) $R_b = 33\,mm$. The natural frequencies of the resonator have been computed with the FEM in COMSOL. It has been proposed to analyse the first resonance that corresponds to oscillation of the hollow sphere and the solid base fixed at its bottom side with respect to the ratio between the height of the sphere enclosure h in the cylindrical base and external radius of the sphere $\widehat{R}$. The selected mode shape of the resonator is shown in Figure 5 where displacement of the resonator components is exaggerated to demonstrate vertical direction of the total displacement. The mesh independence study was conducted on a base with smallest radius, and it was found that with elements of maximum characteristic size 1.7 mm the natural frequency variation converged within 1%.

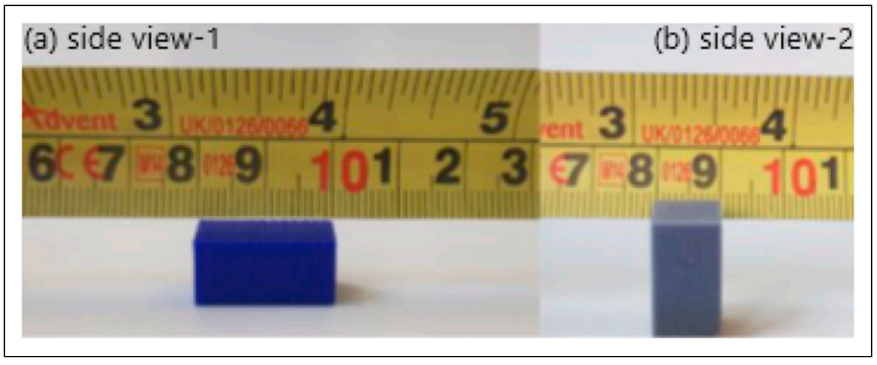

Figure 3. 3D-printed sample made with ABS filament: (a) side view-1 and (b) side view-2.

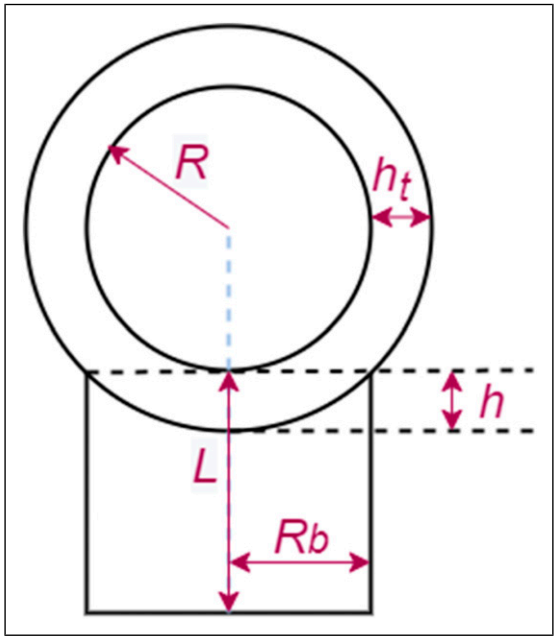

Figure 4. Geometry of the hollow sphere resonator.

Figure 6 demonstrates the change in natural frequency of the resonator with respect to dimensionless displacement of the sphere ($h/\widehat{R}$) into the cylindrical base where h is constrained by h_{max} given by equation (1).

An empirical log-based fit function dependant on dimensionless parameter $h/\widehat{R}$ with $0 < h \leq h_{max}$ is proposed for determining the first natural frequency of the resonator tuned to the third bending mode of the host structure-fixed beam. The fit is given by

$$f\left(h/\widehat{R}\right) = A\log\left(h/\widehat{R}\right) + B, \tag{2}$$

where the fit coefficients A, B and the coefficient of determination r^2 are given in Table 3. The coefficients have been computed in MATLAB with the function polyfit.[24] The coefficient r^2 defines how well the empirical relationship fits the numerical results where value close to one indicates accurate representation of the resonator first natural frequency as a function of the dimensionless parameter h/R.

Figure 6(a) demonstrates the logarithmic trend in the change of natural frequency. All cylindrical supports demonstrate similar effect of the sphere-base contact area on the natural frequencies for the low contact areas ($h/\widehat{R} < 0.001$) as shown in Figure 6(b). Both linear and logarithmic representations are provided in Figure 6. The linear scale illustrates the absolute variation of intrinsic frequency with base height and outer radius ratio, whereas the logarithmic scale highlights sensitivity trends for small parameter changes. For all cases the increase in the contact area results in increase of the resonator natural frequency. This is consistent with the idea that the contact between the sphere and the base can be considered as a form of stiffness, where an increase in this stiffness raises the natural frequency of the sphere's oscillation. It is also noted that at higher frequency for $h/\widehat{R} > 0.01$ the effect of the base dimension impacts the stiffness of the contact and the change in the natural frequency of the resonator differs significantly for the different base parameters. It is also noted that support with smaller radius gives smaller range of the natural frequencies as the contact area ratio is limited by the base diameter.

Table 2. Mechanical properties of ABS at ambient temperature.

Material properties	Young's modulus [Pa]	1.45 E + 09
	Poisson's ratio [-]	0.35
	Density [kg/m^3]	950
	Loss factor	2.18E−02

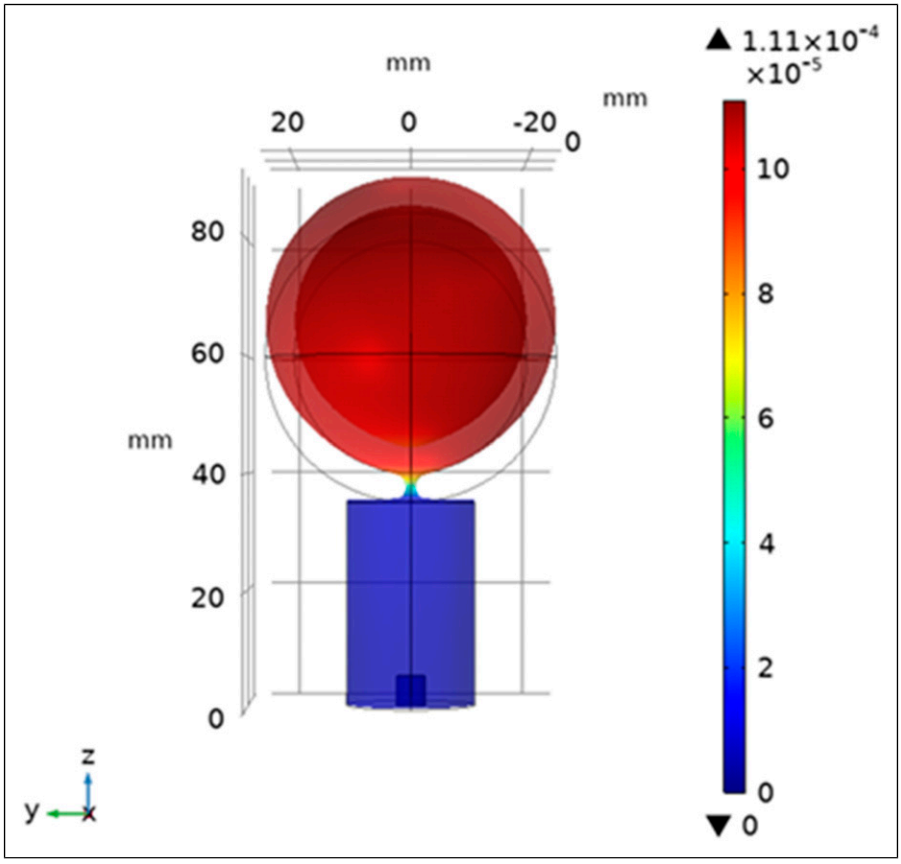

Figure 5. Total displacement for mode shape of the resonator with base $R_b = 11$ *mm* at 838.6 *Hz*.

Taking into the account similar behaviour of the resonator with different bases in the proximity to the 3rd bending mode of the main structure (fixed beam) and need for reducing computational time, the radius of the resonator base is selected as $R_b = 11$ mm for further studies of the resonator effect on the modal response of the beam.

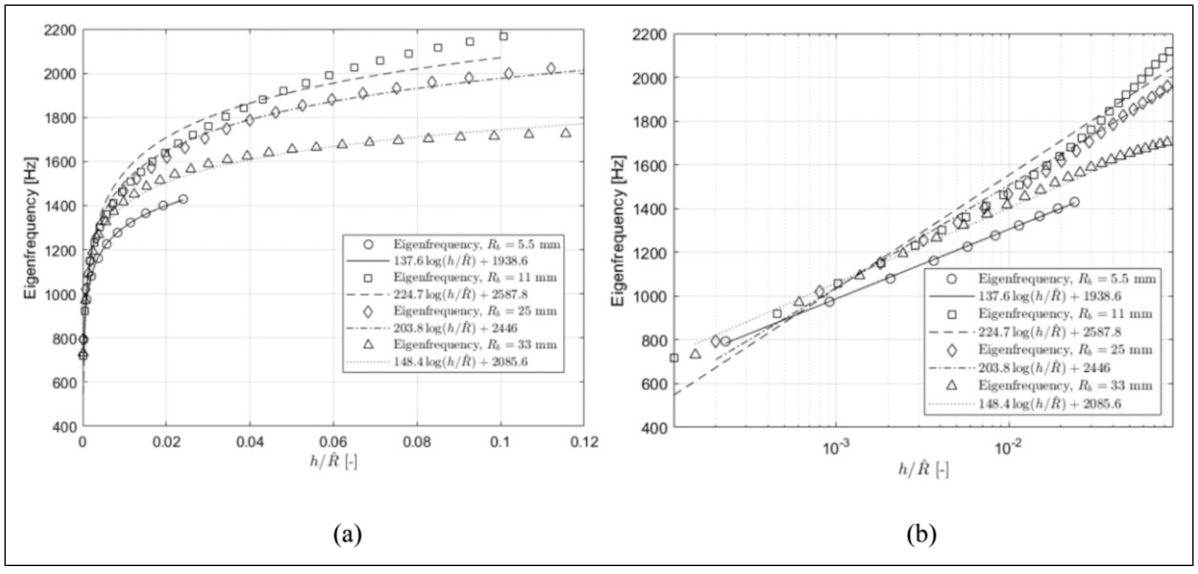

Figure 6. Eigenfrequency of hollow sphere resonator with 4 different cylindrical bases: (a) log-based fit in $h/\widehat{R}$ linear scale and (b) log-based fit in $h/\widehat{R}$ log scale.

Table 3. The log-based fit coefficients.

		Coefficients		
		A	B	r^2
Base radius, R_b, mm	5.5	137.6	1938.6	0.9993
	11	224.7	2587.8	0.9707
	25	203.8	2446	0.994
	33	148.4	2085.6	0.992

Finite element modelling of beam-resonator system

In this section, the dynamic response of single and multiple resonators, which has been introduced in the section of Low-frequency Resonator, placed on the main structure has been analysed with FEM with the aim to develop a novel approach to control beam's bending mode. The resonators have been positioned in close proximity to the antinodes and the nodes of the targeted bending mode to investigate influence of the resonator location on the reduction of the modal response.

Throughout this research, the method of FRF amplitude calculations in the frequency sweep analysis has adopted the inertance calculation which uses the acceleration and the excitation force. In all numerical simulations the excitation impact has been applied to the centre of the beam through the vertical direction.

Numerical simulation of single resonator performance attached to the main structure

The impact of a single resonator on the beam dynamic response is studied in this section by placing the resonator at three locations near either the nodes or the antinodes of the third bending mode.

According to the beam theory,[25] the antinode of the 3rd bending mode is expected at the centre of the beam (see Figure 7) and around 130 mm away from the centre, whereas the node is expected to be around 70 mm from the centre of the beam.

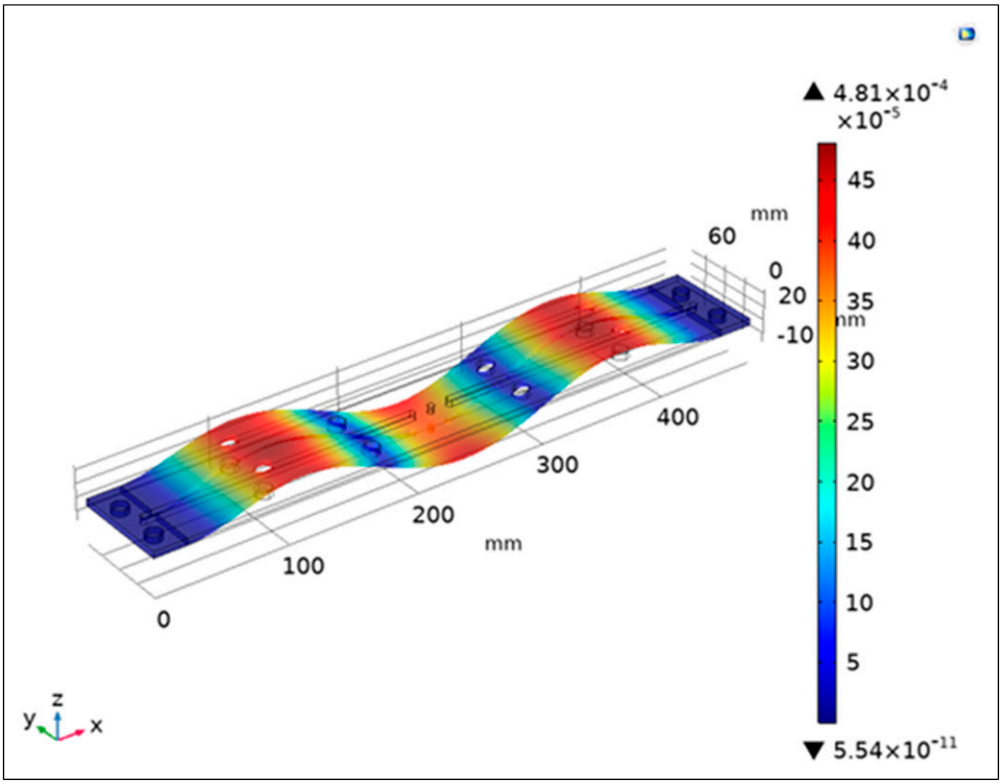

Figure 7. The third bending mode of the main structure at 763.11 Hz with the spatial deflection representation.

To simulate the frequency response of the structure at the 3rd mode of the beam the excitation is placed at the centre of the beam which is the antinode of the beam 3rd mode. In the following analysis, the beam coordinate is defined such that the $x-$ axis coincides with the beam length and $x = 0$ mm denotes the beam midpoint, where the excitation force is applied. The third bending mode features a displacement antinode at $x = 0$ mm and symmetric nodes at approximately $x = \pm 70$ mm, while secondary antinodal positions occur at $x = \pm 130$ mm. All resonator placements in this section are therefore expressed relative to the beam centre.

It is noted that the natural resonance frequency of the additively manufactured resonator (see Figure 5) is at 838 Hz, which is higher than the corresponding bending resonance of the bare beam (see Figure 7), which is at 763 Hz. This mismatch is consistent with locally resonant metamaterial design principles, where the absorber resonance does not need to match the host structure mode frequency exactly. Instead of this, slightly higher resonance frequency promotes the formation of coupled modes and the emergence of a stop band around the interaction region. Similar mismatch between host structure modes and attached resonator modes has been reported previously by Sun et al.[5] where the resonator frequency lies above the structural mode but contributes to the shift of the mode and the formation of local resonance induced attenuation in the whole structure.

Figure 8 illustrates changes in the inertance through a frequency sweep analysis for single resonator cases. It can be noted that the first mode of the beam observed at around 140 Hz has been shifted slightly by only 3.5% indicating the negligible effect of the resonator total mass on the dynamic response of the beam.

The second mode of the system is expected at around 420 Hz has not been efficiently excited due to the location of the dynamic load coinciding with node of the 2nd bending mode. Placement of the single resonator at the antinodes is expected to have more effect on the main structure's third bending mode, leading to a larger mode frequency shift as shown in Figure 8. The mode has been shifted to a lower frequency, while the natural frequency of the resonator has appeared at higher frequency. This behaviour is similar to that reported by Colquitt et al.[26] where attached mass–spring resonators result in frequency band gaps that can be used to control the structural mode. The corresponding eigenfrequency of the beam is shifted by approximately 6% to 720 Hz for the single resonator placed at the centre of the beam, while placement at the node of the mode is produced smaller shift (by around 3% to 745 Hz).

Numerical simulation of resonator array attached to the main structure at antinodes

Multiple resonator placements, involving two and three resonators symmetrically attached to the main structure at the antinodes of the third bending mode, have been considered in this section. Depending on the number of resonators, the centre of the main structure has been either occupied by a resonator or left unoccupied; according to this, even numbers of resonators leave the centre of the beam unoccupied. Including a resonator at the excitation location in the three-resonator

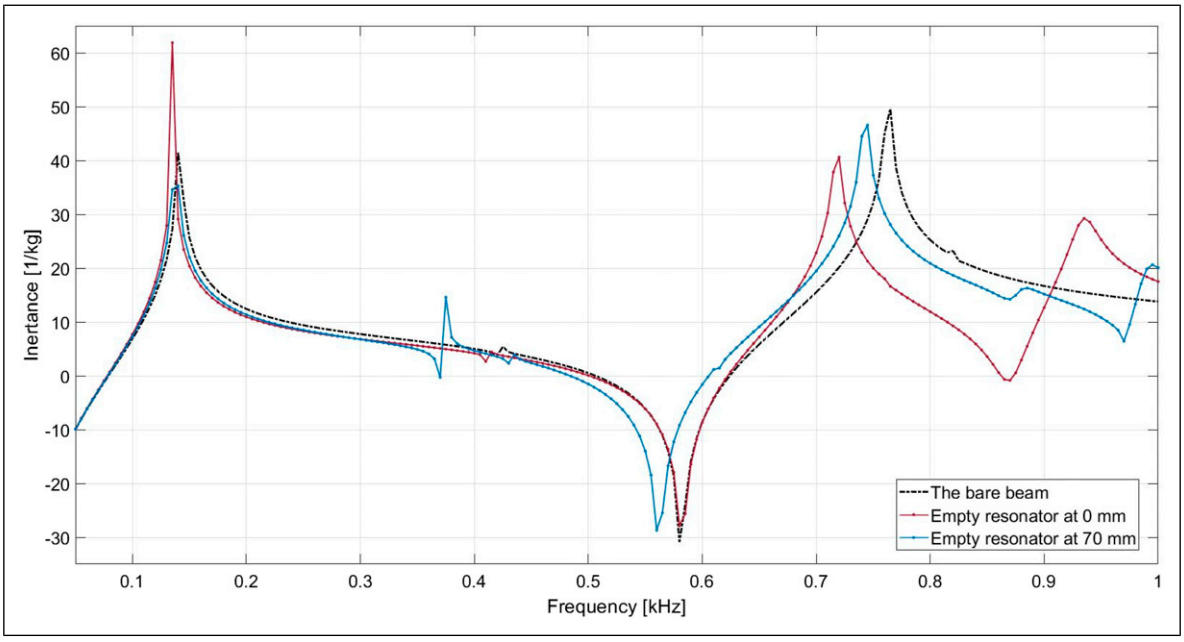

Figure 8. Frequency response of the single resonator placement on the bare beam.

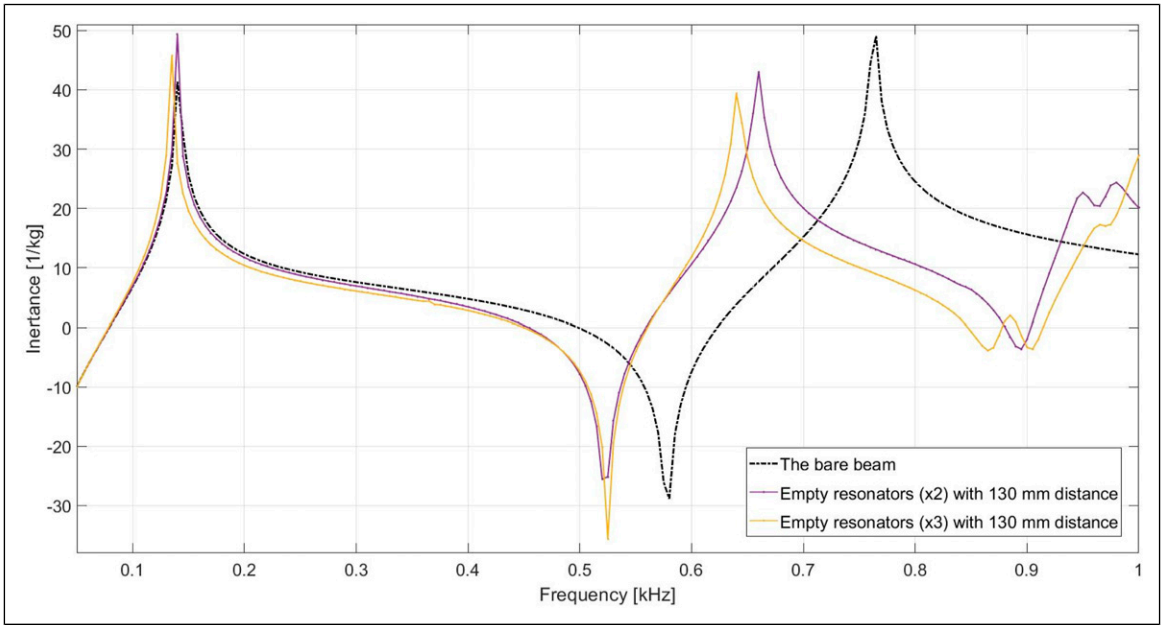

Figure 9. Frequency response of the single resonator placement on the bare beam.

case allows to evaluate the extent to which the resonator interferes with the applied force and influences the resulting frequency response. It is noted that the added mass effect of the array on the beam is expected to have negligible impact on the low-frequency response below the third bending mode. This is supported by largely unchanged response at the first bending mode as shown in Figure 9.

In Figure 9, the resonators are distributed within a 130 mm distance from the centre of the beam. For the two-resonator arrangement, the coupled resonator-beam mode is computed at approximately 675 Hz resulting in a shift of the eigen-frequency of the main structure by approximately 13% and widening a frequency gap previously observed for a single resonator in Figure 8. Placing three resonators widens the frequency gap shifting the third bending mode to 640 Hz by approximately 16%. The increase in the frequency gap between the third bending mode and the natural frequency of the coupled resonators is in alignment with findings in the literature.

Experiment

To validate the results obtained with numerical model, an experimental rig has been set up to perform frequency sweep analysis using traditional shaker-damper tests.[13] Excitation from the shaker has been applied to the beam at Point 1 using a stinger in the direction opposite of gravity, as illustrated in Figure 10(a). The Frequency Response Function (FRF), referred to as inertance in the section of Finite Element Modelling of Beam-Resonator System, is calculated using data from a force transducer (model Dytran 1053VX) which has been placed directly on the shaker (Point 1), and an accelerometer (model Dytran 3225F) which has been positioned 5 mm away from the centre of the beam (Point 2) as shown in Figure 10(b). The resonators have been mounted on the beam through the slit as shown in Figure 10(c). It is noted that in case of experimental FRF, averaging over five samples as well as moving average filter have been applied to eliminate the noise when plotting data in MATLAB version 2022b.[27]

In the experimental setup shown in Figure 10, the beam was clamped at both ends using rigid steel vices with high stiffness. This produces an effective fixed-fixed boundary condition for the experimental setup. This constraint was simulated in the FEM model discussed in section 3. The compliance of the clamping assembly was measured to be negligible compared to the bending stiffness of the beam, ensuring equivalence between simulation and experiment.

The data has been collected and processed by PicoScope 2000. The beam is identical to that from the section of Low-frequency Resonator with fixed-fixed-end conditions and made of structural steel with properties similar to those shown in Table 1. It has been designed with holes along its length to accommodate different mounting options, as shown in Figure 1. The response of the structure has been evaluated using the frequency sweep excitation from 10 Hz to 4 kHz with step of 2 Hz and sampling rate of 100 kHz.

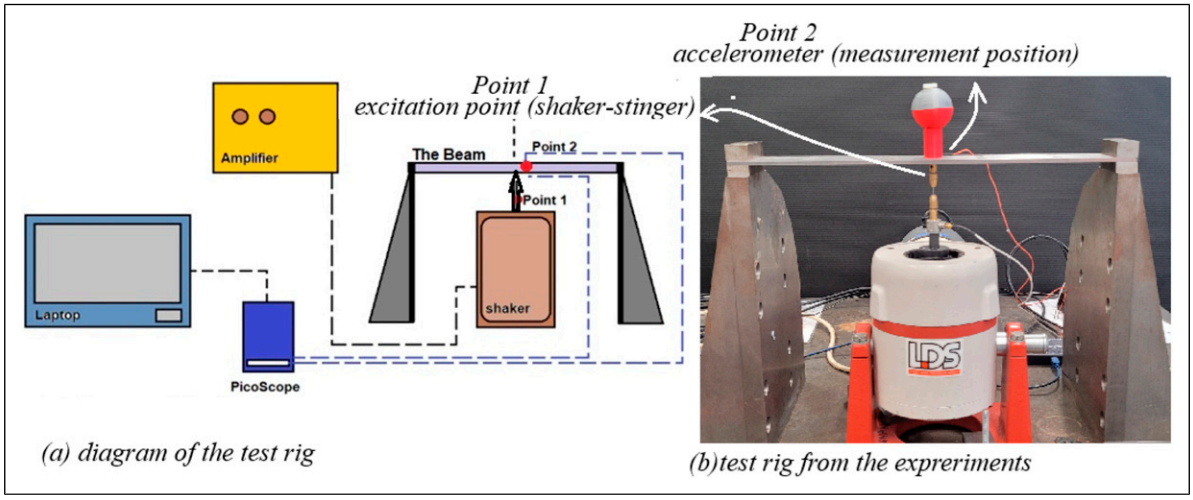

Figure 10. Experimental analysis rig: (a) the diagram of the test rig and (b) the test rig in the laboratory.

The bare beam test has produced results similar to those obtained in numerical simulations (see the section of Low-frequency Resonator). The first three bending modes are recorded at 130 Hz, 395 Hz, and 725 Hz as can be seen in Figure 11. As in the case of the numerical simulation, the second bending mode has not been effectively excited since the source is located at the node of this mode.

Single and multiple resonator performance

Single and multiple resonator attachments have been experimentally studied to validate the numerical results from the section of Finite Eelement Modelling of Beam-Resonator System. Figure 11 displays the frequency response of the beam for single resonator placement cases identical to those studied numerically in the section of Finite Element Modelling of Beam-Resonator System. As in the case of numerical simulation, single resonator placement is not significantly impacted the response of the beam around the first bending mode (around 140 Hz) and the coupling between the resonator and the beam is observed within the frequency range of 700–800 Hz. For the antinodes, the

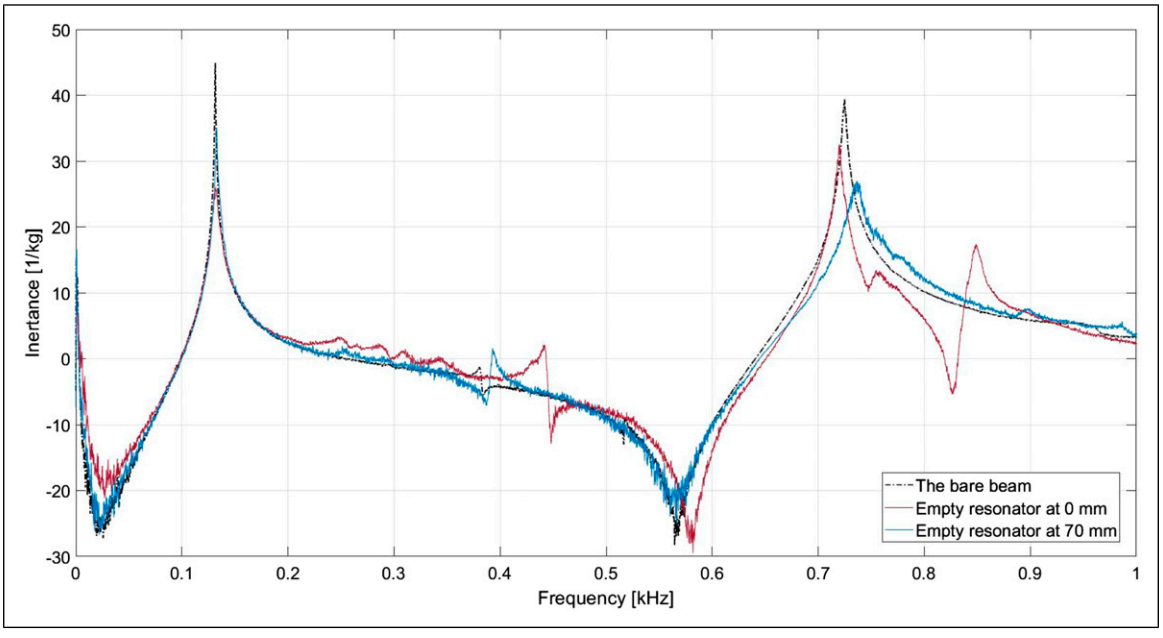

Figure 11. Experimentally analysed frequency response analysis of the single resonator attachment on the beam.

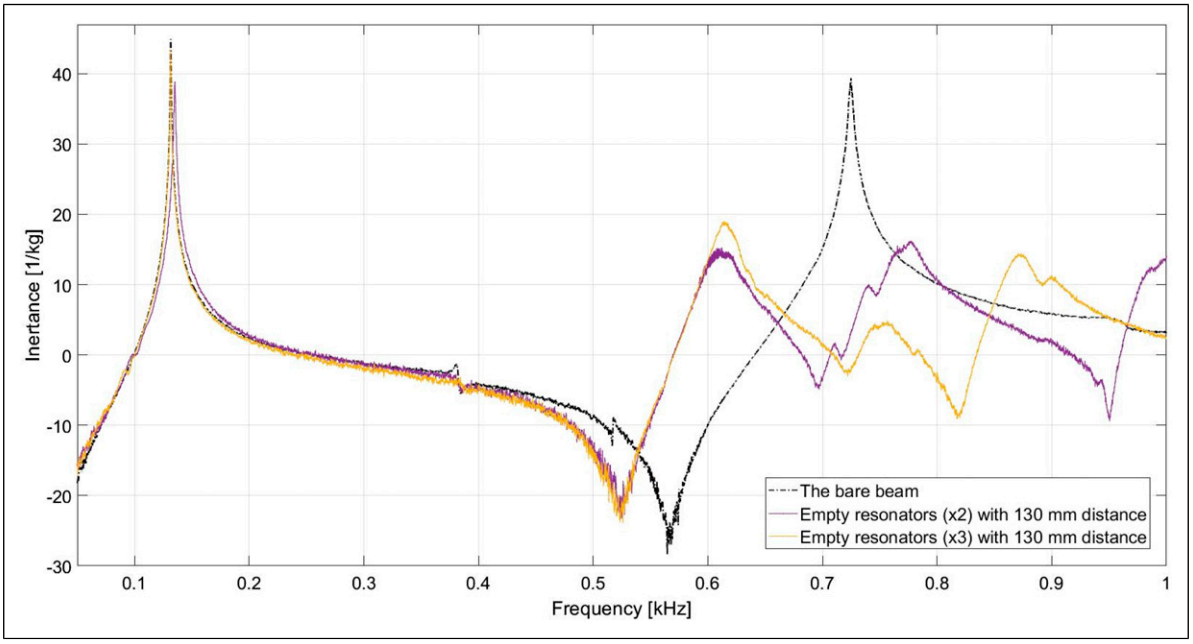

Figure 12. Experimentally analysed frequency response analysis of the multiple resonator attachments on the beam.

resonance of the system is shifted, although on a much smaller scale, by approximately 1% to 720 Hz (centre-positioned resonator). It is noted that at the antinode, it is possible to excite resonance associated with the resonator and expected between 800 and 900 Hz as seen in Figure 11.

Figure 12 depicts the impact of multiple resonators on the beam in configurations identical to those in th section of Numerical Simulation of Resonator Array Attached to the Main Structure at Antinodes. The effect of coupled resonators is observed between 600 Hz and 1000 Hz. The third bending mode of the beam is shifted to a lower frequency while the magnitude of the FRF is significantly reduced in all resonator arrangement cases. In case of two resonators, the frequency of the bending mode is shifted by approximately 16% to 610 Hz. Similar results are observed for the three-resonator case with shift of the main structure's natural frequency to 615 Hz.

These results are consistent with the numerical simulations of multiple resonator attachments where the frequency of the 3rd bending has been shifted by a similar amount (13–16%) and both configurations of the resonators provide similar responses.

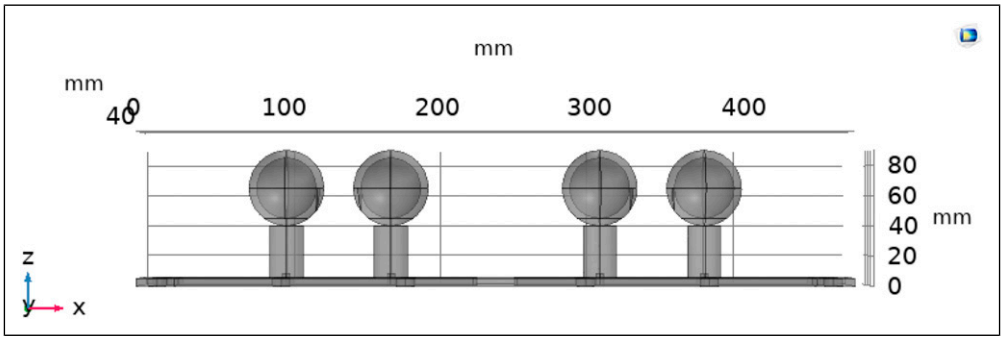

Figure 13. Four-resonator placement with the 70 mm distance from the centre of the beam ($x = 0$ mm).

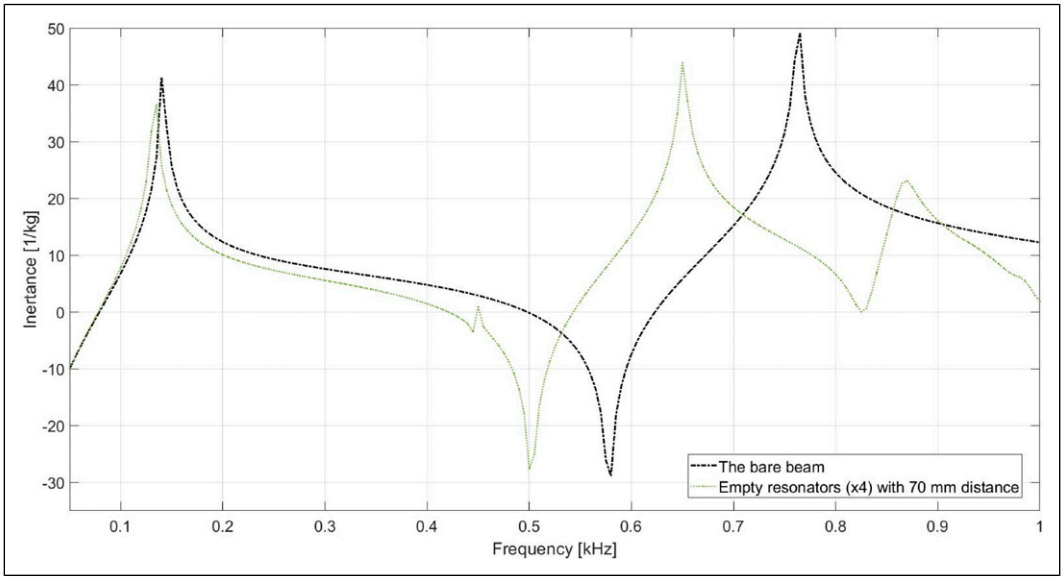

Figure 14. Frequency response of the beam with an array of resonators attached near nodes and antinodes of the main structure.

Effect of node and antinode on the performance of array of resonators

To evaluate the effect of node and antinode on the performance of the array of resonators, four dampers have been placed on the beam with the 70 mm distances symmetrically with respect to the centre of the beam as shown in Figure 13. In this arrangement, the array of resonators is located near both the node and the antinode positions of the main structure.

The numerical simulation of the frequency response of this structure demonstrated in Figure 14 shows that the frequency of the third bending mode is shifted by approximately 15% to 650 Hz which is similar to that obtained for the three-resonator case located at the antinodes only. This indicates that the resonators attached at the nodes have minor impact on the overall performance of the array. Similar observations are made for a single resonator (see section Numerical Simulation of Single Resonator Performance Attached to The Main Structure).

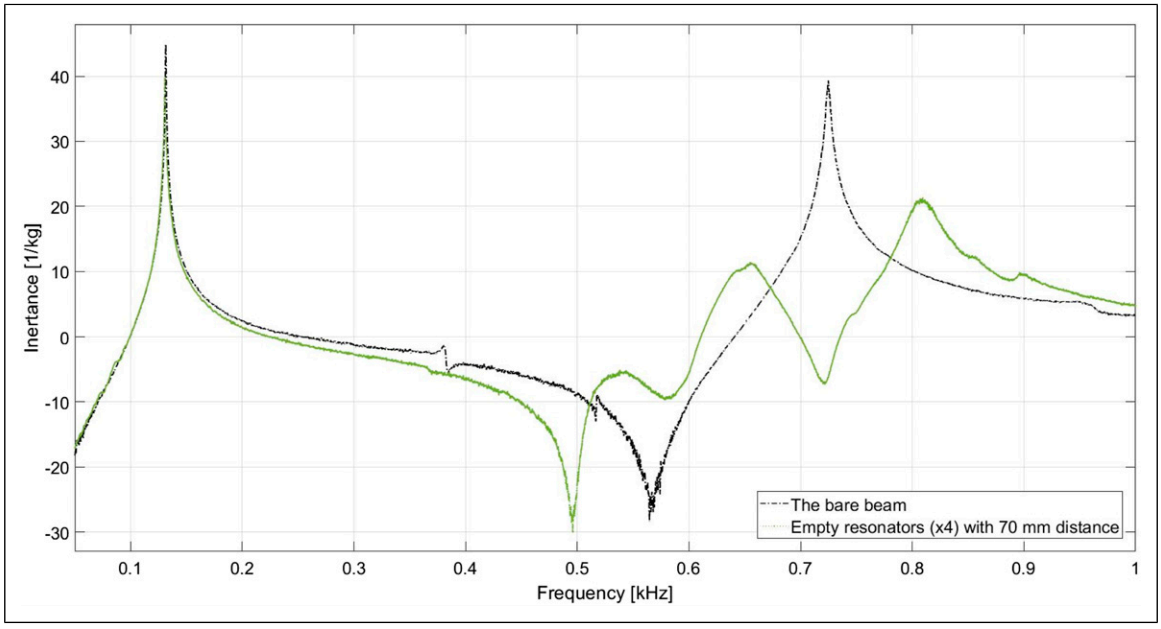

Figure 15. Experimentally analysed frequency response analysis of the 70 mm distance applied multiple resonator attachments on the beam.

Performance of four-resonator arrangement is validated with the experiment as shown in Figure 15. As in the numerical simulation, the eigenfrequency of the third bending mode is shifted by 9.5% to 655 Hz. Additionally, as in the case of tests for two and three resonator arrays, the FRF amplitudes at the eigenfrequency region are reduced, as supported by the findings in Demiryurek.[28]

Both simulation and experiment show that the resonator attached at the node of the corresponding bending mode has a negligible impact on the overall performance of the array.

Tunability and low-frequency applicability

Although the experimental setup in this work targets the third bending mode of the main structure at approximately 760 Hz due to the laboratory-scale constraints, the proposed resonator design is inherently scalable to lower frequencies. The local resonant frequency is governed by the stiffness at the connection between spherical cavity cylindrical support:

$$f_r \propto \sqrt{k_{eff}/m_{eff}} \tag{3}$$

which means that modifying stiffness of the connection (k_{eff}) enables tuning to significantly lower range of frequencies (100–300 Hz) relevant for wide range of engineering structures.

Resonators partially filled with granular material

Granular structure dissipation mechanism

The enhanced damping observed in the granular-filled resonator originated from strongly nonlinear interactions between particles and cavity wall. These mechanisms differ from the linear resonance-based damping of the empty resonator and give rise to broadband, amplitude-dependent damping of the whole structure. In order to clarify these effects, a theoretical framework based on Hertzian contact mechanics, coordination number and collision related energy dissipation is presented in this subsection.

Hertzian normal and tangential contact forces. The interaction between the granular filling and the resonator walls is governed by the short duration of viscoelastic contacts and frictional sliding. These interactions within the granular structures dissipate energy through the particle–particle and particle–cavity wall relations. According to the Hertzian Contact Theory, these interactions generate strongly amplitude-dependent normal and tangential forces, which leads to irreversible momentum exchange and energy loss.[29] Tangential contact behaviour within the granules influences the energy dissipation since the friction coefficient and sliding, slipping motions, specifically in the high friction coefficient impacts. In the case of low friction coefficients within the granules, energy dissipation is mostly dominated by the normal impacts within the granular contacts. In terms of the granular packing, these contacts are tracked between the particle–particle and particle–wall relations over the transient force evolutions.[30] DEM or DEM-FEM coupled analysis[31] can provide detailed insight into granular dynamics, but such analysis is computationally expensive due to the tracing over each granule per contacts. The objective of the present research is to verify the energy dissipation impact and damping enhancement offered by the granular structure through experimental study by placing partially filled resonators on the main structure rather than a fully developed granular structure solver.

Energy dissipation in granular-filled resonators arises mainly from two mechanisms: viscoelastic impact losses and frictional sliding. Among these, the coefficient of restitution (e) plays a central role because it defines the proportion of kinetic energy preserved after a collision. A value close to one corresponds to an almost elastic impact with minimal dissipation, whereas values closer to 0 indicate inelastic behaviour with significant energy loss. Material stiffness affects this parameter: stiff materials such as steel typically exhibit high restitution coefficients and therefore dissipate less energy per collision. In contrast, granular damping applications generally benefit from media with moderate to low restitution coefficients, since these promote stronger inelastic impacts and higher momentum loss. Previous studies consistently show that particle dampers operate most efficiently within the low-to-moderate restitution regime.[14,32]

The granular medium used in the present study exhibits a restitution level in this favourable regime, which explains the noticeable enhancement in modal damping observed in the experiments. Another specific parameter that governs the energy dissipation is the coordination number[28,33] which is the average number of active contacts per particle in the packed granules in a cavity and directly depends on the granular material filling fraction. The coordination number controls the formation and collapse of the internal force chains, which in turn determine the dominant damping mechanisms. DEM and experimental studies identify three regimes according to their solutions and damping variations. Particles interact with the cavity walls

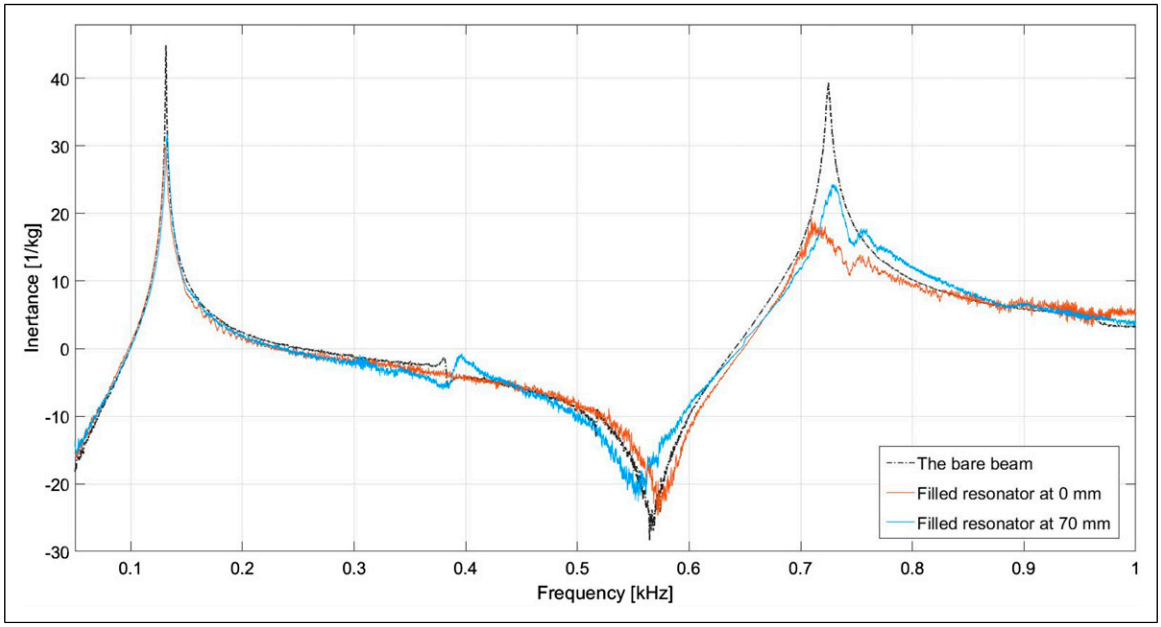

Figure 16. Frequency response of the main structure with single resonator filled with 10% metal particles.

primarily in the case of low filling ratios and dissipation is dominated by the normal impact losses mostly with the particle–particle contacts. The second variations are when the cavity is filled with granules at a moderate level where the granules exhibit increased mobility and frequency particle–particle collisions.[31] This regime combines the impact dissipation, frictional sliding, and is known as the highest damping efficiency area under low to moderate level of excitation levels. Lastly, at high filling levels, particles move collectively with low relative motion to each other which reduces the collision and damping. In this study moderate level 10% filling fraction is used which supports the damping enhancement in the measured frequency range.

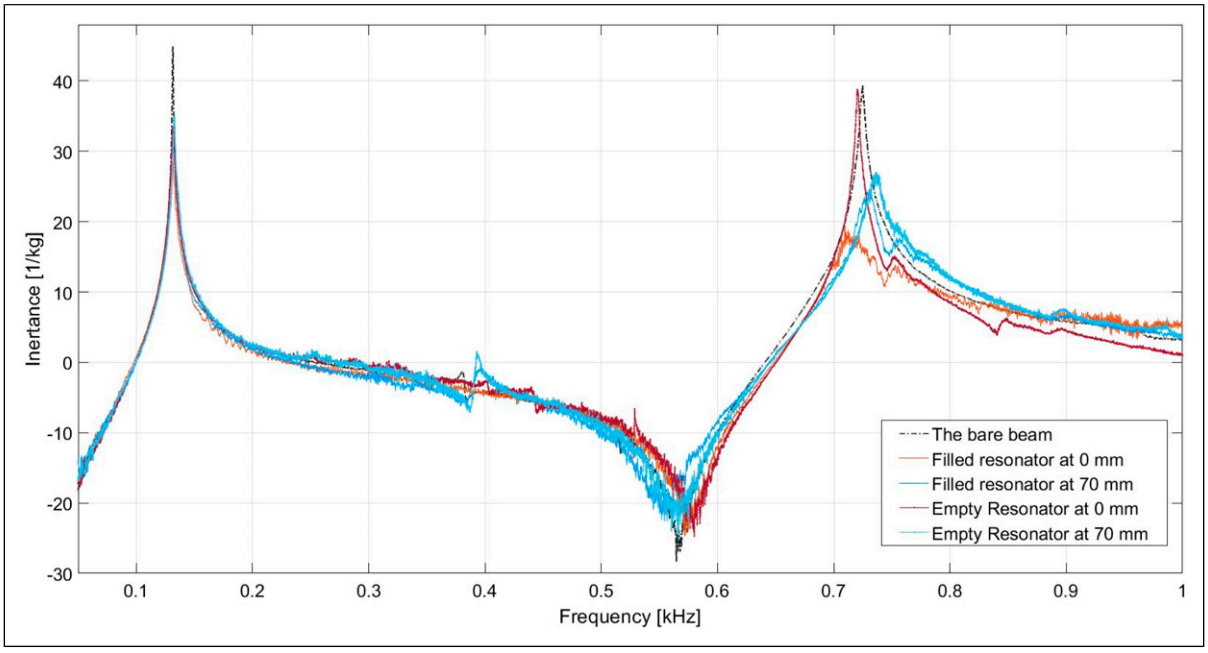

Figure 17. Comparison of empty and filled single resonator attachments on the beam.

Partially filled resonator example

Placement of granular material in the damper cavity has been mentioned in Section 1 as an additional damping mechanism related to the interactions between granules and the cavity walls. In this paper, in order to study the effect of granular medium on the frequency response of the main structure, 10% of a single resonator cavity volume has been filled with metallic spherical particles with a diameter of 1.59 mm. The mass of the metal particle filling is 26.3 g which is much smaller than the mass of the main structure and is not expected to significantly impact the first and the second bending modes. The filled resonator is placed at two locations, as in the case of the empty resonator (0 mm and 70 mm) placement to assess the impact of granular filling on the frequency response of the main structure.

Figure 16 illustrates the impact of granular structure placement in the resonating damper cavity and the cases are identical to those from the previously discussed single resonator placement studies shown in Figure 11. Examining the data trends in the figure, it is evident that the centrally placed filled resonator results in a shift of the third bending mode by 2% (shifted at 710 Hz) compared to the beam's response. When the filled resonator is placed at 70 mm from the centre of the beam, it shifts the resonance of the whole structure by 0.8% (at 730 Hz). In addition to the reduced local resonance, the presence of granules in the damper cavity has led to a 45% reduction in inertance amplitude, indicating that the granules have contributed to damper performance.

Figure 17 includes the response of a single empty resonator to enable direct comparison with the partly granular-filled configuration. The results show that while the empty resonator already contributes to a reduction in the third bending mode amplitude, the addition of granular material provides further attenuation. This enhanced suppression is attributed to impact and friction-induced energy dissipation within the granular medium, which introduces nonlinear damping mechanisms not present in the empty resonator.

Conclusion

This paper explores the use of resonators with granular filling in altering the modal response of the main structure. The study models an unconventional hollow-spherical resonator using a parameter-based analytical approach. It also examines the production and material characterisation of the resonator. Experimental and numerical analyses assess the resonators' effects on external energy absorption across a frequency range up to 1 kHz, considering both single and multiple resonator configurations. A key finding is the emergence of relatively wide frequency gaps of up to 200 Hz in multiple resonator setups, demonstrating the efficiency of lightweight structures in low-frequency regime. Granular materials filled resonator further improved the efficiency resulting in a 45% reduction of FRF amplitude of the main structure response. This supports the potential of particle-filled resonators for damping, highlighting the need for further study of the effect of granular materials within resonators to enhance their performance.

ORCID iD

Sifa Gul Demiryurek https://orcid.org/0000-0002-9888-0581

Funding

The authors disclosed receipt of the following financial support for the research, authorship, and/or publication this article: This study was funded by the Republic of Turkey Ministry of National Education.

Declaration of conflicting interests

The authors declared no potential conflicts of interest with respect to the research, authorship, and/or publication of this article.

References

1. Mead DJ. Criteria for comparing the effectiveness of damping treatments. *Noise Control* 1961; 7: 27–38.
2. Liu J, Guo H and Wang T. A review of Acoustic metamaterials and phononic crystals. *Crystals* 2020; 10: 305.
3. Harne RL, Song Y and Dai Q. Trapping and attenuating broadband vibroacoustic energy with hyperdamping metamaterials. *Extreme Mech Lett* 2017; 12: 41–47.
4. Lu Z, Wang Z, Masri SF, et al. Particle impact dampers: past, present, and future. *Structural Control and Health Monitoring2018* 2058; 25: 1–25.
5. Sun H, Du X and Pai PF. Theory of metamaterial beams for broadband vibration absorption. *J Intell Mater Syst Struct* 2010; 21: 1085–1101.
6. Pai PF. Metamaterial-based broadband elastic wave absorber. *J Intell Mater Syst Struct* 2010; 21: 517–528.

7. Demiryürek ŞG. *Introduction to the metamaterials*. Zenodo, 2025, p. 77. https://doi.org/10.5281/zenodo.17447584
8. Nouh M, Aldraihem O and Baz A. Vibration characteristics of metamaterial beams with periodic local resonances. *Journal of Vibration and Acoustics, Transactions of the ASME* 2014; 136: 1–12.
9. Surjadi JU, Gao L, Du H, et al. Mechanical metamaterials and their engineering applications. *Adv Eng Mater* 2019; 21: 1–37.
10. Diaz AR, Haddow AG and Ma L. Design of band-gap grid structures. *Struct Multidiscip Optim* 2005; 29: 418–431.
11. Pai PF, Peng H and Jiang S. Acoustic metamaterial beams based on multi-frequency vibration absorbers. *Int J Mech Sci* 2014; 79: 195–205.
12. Demiryurek SG and Krynkin A. Low-frequency broadband vibration dampers from nonlinear structures with metamaterial properties. *ACOUSTICS 2021*. Institute of Acoustics (IOA), 2021. doi:10.25144/13760.
13. Saeki M. Analytical study of multi-particle damping. *J Sound Vib* 2005; 281: 1133–1144.
14. Wong CX, Spencer AB and Rongong JA. Effects of enclosure geometry on particle damping performance. *Structural Dynamics and Materials Conference*. The American Society of Mechanical Engineers, 2009, pp. 1–16. doi:10.2514/6.2009-2689.
15. Demiryurek SG and Krynkin A. Low-frequency broadband vibration damping using the nonlinear damper with metamaterial properties. *DAGA 2021*. Deutsche Gesellschaft für Akustik e.V. (DEGA), 2021, pp. 94–96.
16. Van Ophem S, Van De Walle S, Deckers E, et al. Efficient vibro-acoustic identification of boundary conditions by low-rank parametric model order reduction. *Mech Syst Signal Process* 2018; 111: 23–35.
17. Hussein MJ and Frazier MJ. Metadamping: an emergent phenomenon in dissipative metamaterials. *J Sound Vib* 2012; 332: 4767–4774.
18. Pai PF and Huang G. Design of wide- and multistopband acoustic metamaterials. In: *Theory and design of acoustic metamaterials*. SPIE Press, 2015, pp. 137–172. https://doi.org/10.1117/3.2199731.ch5
19. Galeja M, Hejna A, Kosmela P, et al. Static and dynamic mechanical properties of 3D printed ABS as a function of raster angle. *Materials* 2020; 13: 297.
20. Zieliński TG, Opiela KC, Pawłowski P, et al. Reproducibility of sound-absorbing periodic porous materials using additive manufacturing technologies: round robin study. *Addit Manuf* 2020; 36: 1–33.
21. Demiryurek SG. Evaluation of dynamic properties in ABS and PLA thermoplastics across frequency ranges. *Sci Rep* 2025; 15: 42629.
22. Shubham P, Aggarwal C and Joshi S. Optimisation of process parameter to improve dynamic mechanical properties of 3D printed ABS polymer using Taguchi method. In: *Advanced Research Society For Science And Sociology*, 2018, pp. 21–28.
23. Ahn SH, Montero M, Odell D, et al. Anisotropic material properties of fused deposition modeling ABS. *Rapid Prototyp J* 2002; 8: 248–257.
24. MathWorks United Kingdom. Polynomial curve fitting - MATLAB polyfit. https://uk.mathworks.com/help/matlab/ref/polyfit.html (Accessed 27 May 2025).
25. Thomson WT and Dahleh MD. *Theory of vibration with applications*. 5th ed. Prentice Hall, 1998.
26. Colquitt DJ, Colombi A, Craster RV, et al. Seismic metasurfaces: sub-wavelength resonators and Rayleigh wave interaction. *J Mech Phys Solids* 2017; 99: 379–393. https://doi.org/10.1016/j.jmps.2016.12.004
27. Signal smoothing, (n.d.). https://uk.mathworks.com/help/signal/ug/signal-smoothing.html
28. Demiryurek SG. *Periodically arranged nonlinear passive particle dampers under low-amplitude excitation*. The University of Sheffield, 2022. PhD Thesis.
29. Zdancevičius E, Kačianauskas R and Zabulionis D. Improvement of viscoelastic damping for the hertz contact of particles due to impact velocity. *Procedia Eng* 2017; 172: 1286–1290.
30. Terzioglu F, Rongong JA and Lord CE. Motional phase maps for estimating the effectiveness of granular dampers. *Mech Syst Signal Process* 2023; 188: 110038.
31. Terzioglu F, Rongong JA and Lord CE. Influence of particle sphericity on granular dampers operating in the bouncing bed motional phase. *J Sound Vib* 2023; 554: 117690.
32. Hunt KH and Crossley FRE. Coefficient of restitution interpreted as damping in vibroimpact. *ASME J Appl Mech* 1975; 42: 440–445.
33. Iwata H and Homma T. Distribution of coordination numbers in random packing of homogeneous spheres. *Powder Technol* 1974; 10: 79–83.